Int. J. Electron. Commun. (AEÜ) 178 (2024) 155285

Contents lists available at ScienceDirect

International Journal of Electronics and Communications

journal homepage: www.elsevier.com/locate/aeue

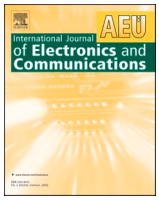

A wideband multi-bit reflectarray antenna with low cross-polarization based on nonradiative dielectric waveguide☆

Wen Wu [a], Kai-Da Xu [a,*], Daotong Li [b], Qiang Chen [a]

[a] Department of Communications Engineering, Tohoku University, Sendai 980-8579, Japan
[b] Research Institute for Sustainable Humanosphere, Kyoto University, Kyoto 606-8501, Japan

ARTICLE INFO

Keywords:
Nonradiative dielectric waveguide
Reflectarray antenna
Multi-bit
Wideband
Low cross-polarization

ABSTRACT

This paper presents a wideband reflectarray antenna (RA) based on a nonradiative dielectric (NRD) waveguide with an inserted metal blade for muti-bit phase quantization. The proposed design eliminates the need of resonant components that typically exist in traditional RAs. Additionally, low cross-polarization is achieved by exciting the appropriate propagation mode in NRD waveguide. The beam scanning performance based on multi-bit phase quantization is verified by a series of static prototypes. Compared to traditional rectangular waveguide RAs, the proposed design possesses collimated beam scanning up to 60° without grating lobes, due to the compact unit cell dimensions. At a collimation beam angle of 20°, a 1-dB gain bandwidth of 18 % is achieved with an aperture efficiency of over 40 % and a cross-polarization level of below −40 dB.

1. Introduction

The beam-scanning ability of reflectarray antennas (RAs) is becoming increasingly important for the satellite communication and 5G/B5G wireless communications [1–3]. X-band beam-steerable RAs offer effective solutions for mitigating signal blockage and rain fading from the environment while ensuring reliable data channels with ultra-high-speed transmission, such as data exchange between data centers [4]. Traditional wideband beam scanning RAs often rely on resonant components and metallic ground structures to reflect electromagnetic (EM) waves [5–8]. The complex multiple substrates with high ohmic losses are typically introduced, leading to high cost [9,10] and decreased efficiency. As an alternative, non-resonant dielectric RAs are gaining attention due to their wideband performance, low metal loss and low-cost fabrication using 3D printing techniques [11–14].

In [11] and [12], a Fresnel zone plate based reflectarray utilizes 3D printed dielectric slabs as phase shifters on a metal ground, achieving a 1-dB gain bandwidth of 20 %. In [13], incident waves are received by a matching layer and propagated through dielectric columns with copper wires for reflection, resulting in a non-resonant design with a 3-dB gain bandwidth of 27 %. In [14], multiple dielectric layers are assembled to receive and propagate the incident wave. Different cutoff frequencies between the dielectric layers are used to manipulate the reflections with a simulated 1-dB gain bandwidth of up to 32 %. However, all these dielectric RAs do not demonstrate the beam scanning ability and complex structures are required to improve the aperture efficiency.

Nonradiative dielectric (NRD) waveguide has emerged as a waveguide structure with low metal loss [15–17]. It consists of a pair of parallel conductor walls with a dielectric slab sandwiched between them. This unique structure allows most of the EM waves to be confined within the dielectric slab, minimizing the ohmic loss in the conductor walls. Furthermore, the presence of the dielectric allows the cross-sectional size of the NRD waveguide to be lower than $0.5\lambda_0$, where λ_0 represents the free space wavelength at the highest operating frequency (i.e., 11.5 GHz). The NRD waveguide possesses the characteristics of the compact size, low metal loss and inherent non-resonance, making it a promising unit cell for the design of wide-angle beam scanning RA with wideband performance.

In this paper, a wideband multi-bit RA with low cross-polarization is proposed based on a new mechanically phase tunable NRD waveguide structure. To the best of our knowledge, it is for the first time to exhibit beam scanning ability while keeping wideband performance for waveguide-type RAs. The precise phase tuning of the unit cell is accomplished by moving the inserted metal blade with multi-bit phase

☆ This work was supported in part by the Program on Open Innovation Platform with Enterprises, Research Institute and Academia, Japan Science and Technology Agency (JST, OPERA, JPMJOP1852).

* Corresponding author.
E-mail address: xu.kaida.q7@dc.tohoku.ac.jp (K.-D. Xu).

https://doi.org/10.1016/j.aeue.2024.155285
Received 6 February 2024; Accepted 6 April 2024
Available online 7 April 2024

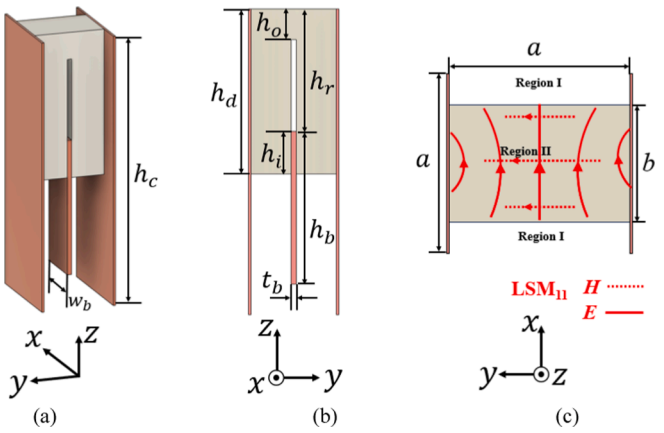

Fig. 1. Structure and the propagation modes of the proposed phase tunable NRD waveguide unit cell. (a) Perspective view. (b) Side view. (c) LSM_{11} mode. The metal is in red orange and the dielectric slab is in grey.

Table 1
Dimensions of The Proposed NRD Waveguide Unit Cell.

Parameter	a	b	h_p	h_b	h_d
Value (mm)	13	10	40	22	27
Parameter	h_o	w_b	ε_r	t_b	h_r
Value (mm)	5	11	2.7	0.8	varied

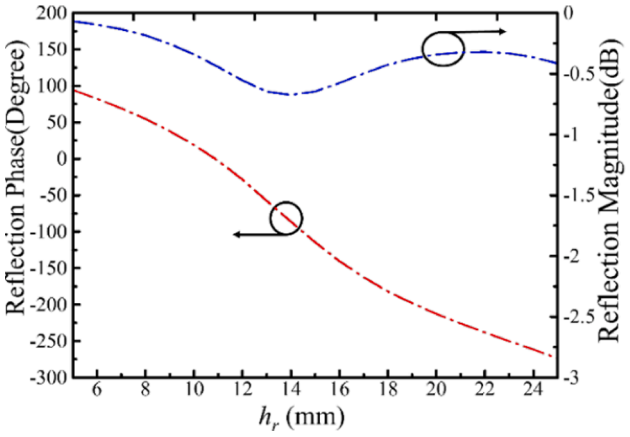

Fig. 2. Simulated reflection coefficient versus blade position h_r at 10 GHz.

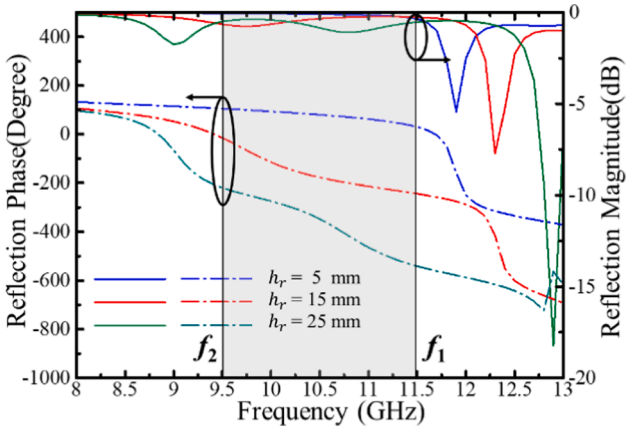

Fig. 3. Simulated reflection coefficient versus frequency with different values of h_r.

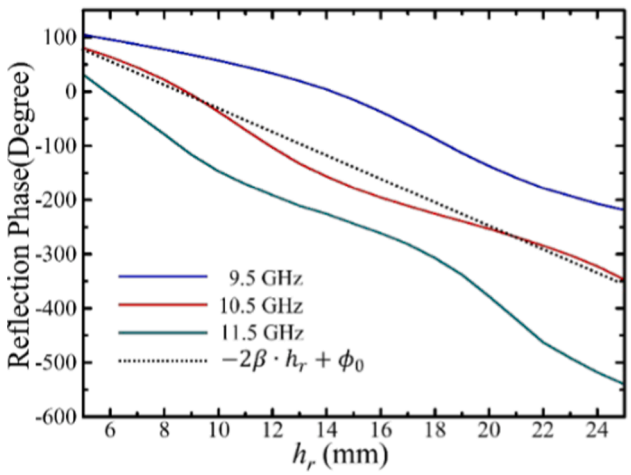

Fig. 4. Simulated reflection phase versus h_r at the low, center and high frequencies within the operating bandwidth.

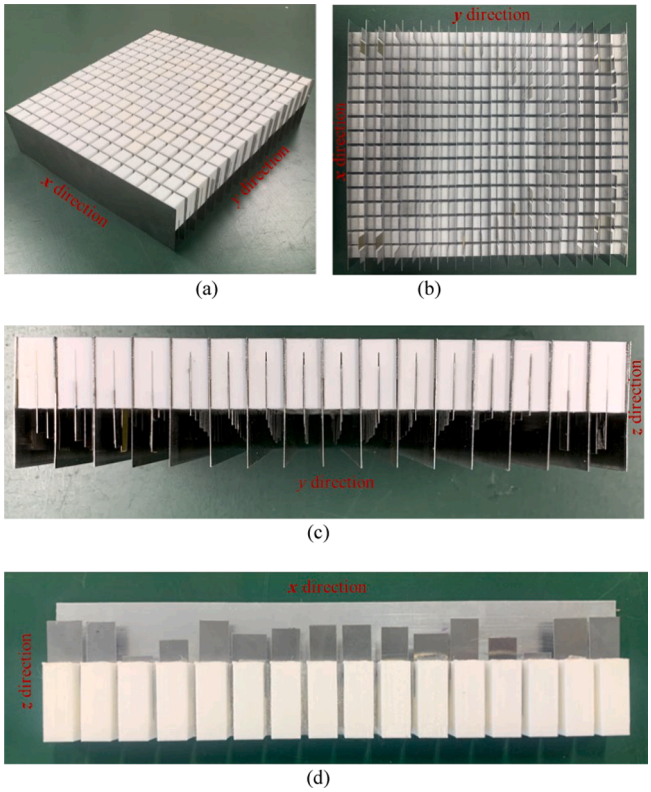

Fig. 5. The prototype of the proposed muti-bit RA. (a) Perspective view. (b) Bottom view. (c) Side view. (d) Internal structure of one column of the RA.

quantization. The prototype of the proposed design with 16 × 16 unit cells is fabricated, which achieves a maximum scanning angle of 60° with a scanning loss of 3.5 dB. The 1-dB gain bandwidth reaches 18 % with an aperture efficiency exceeding 40 % for the collimation beam at 20°.

2. Unit cell of Multi-Bit reflectarray based on NRD waveguide

NRD waveguides offers a significant reduction in metal losses by removing the upper and lower metallic walls, which are major contributors to power dissipation in conventional rectangular waveguides [15–18]. Instead, the NRD waveguide employs a dielectric slab to

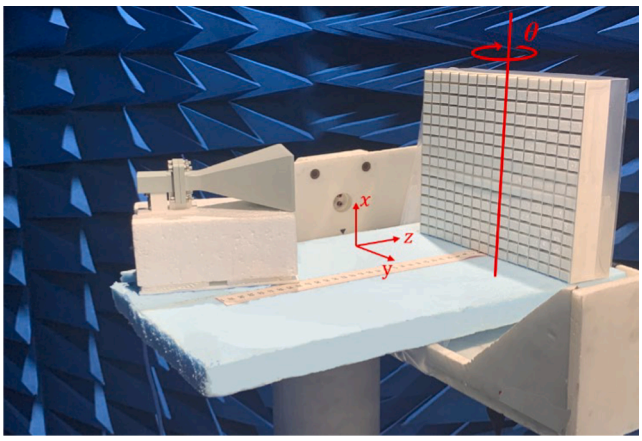

Fig. 6. Measurement setup for H plane of the RA prototype.

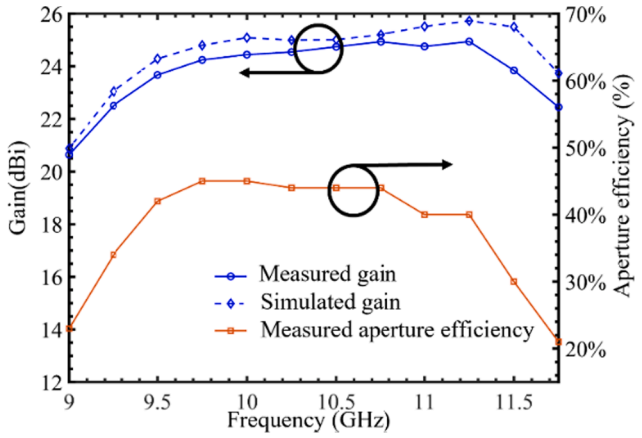

Fig. 7. RA gains and aperture efficiency of collimation beam with $\theta_c = 20°$, $\varphi_c = 90°$.

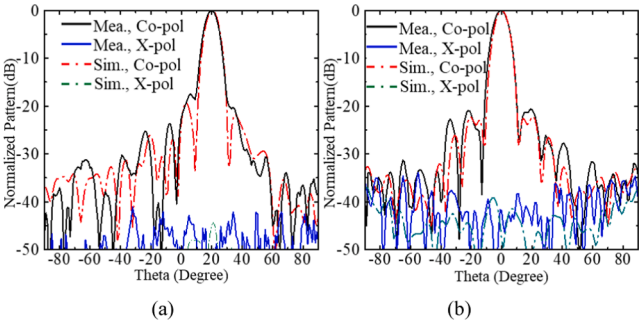

Fig. 8. Comparisons between measured and simulated patterns of the collimation beam with $\theta_c = 20°$, $\varphi_c = 90°$ at 10.5 GHz. (a) H-plane. (b) E-plane.

confine the EM wave which has a lower cutoff frequency than the surrounding air, effectively preventing the propagation of EM waves from the dielectric to the air.

Compared to conventional NRD waveguide, the proposed structure has a deep groove in the dielectric slab where a blade-like conductor sheet is inserted, as shown in Fig. 1. The dominant propagation mode is set to longitudinal-section-magnetic (LSM_{11}) mode [19,20], whose magnetic field is parallel to the longitudinal plane (*xoz* plane). Based on this configuration, the spatial feed incident wave should be set to *x*-polarization. The main part of transversal E-field component of the LSM_{11} mode is parallel to the polarization of the incident wave, and it

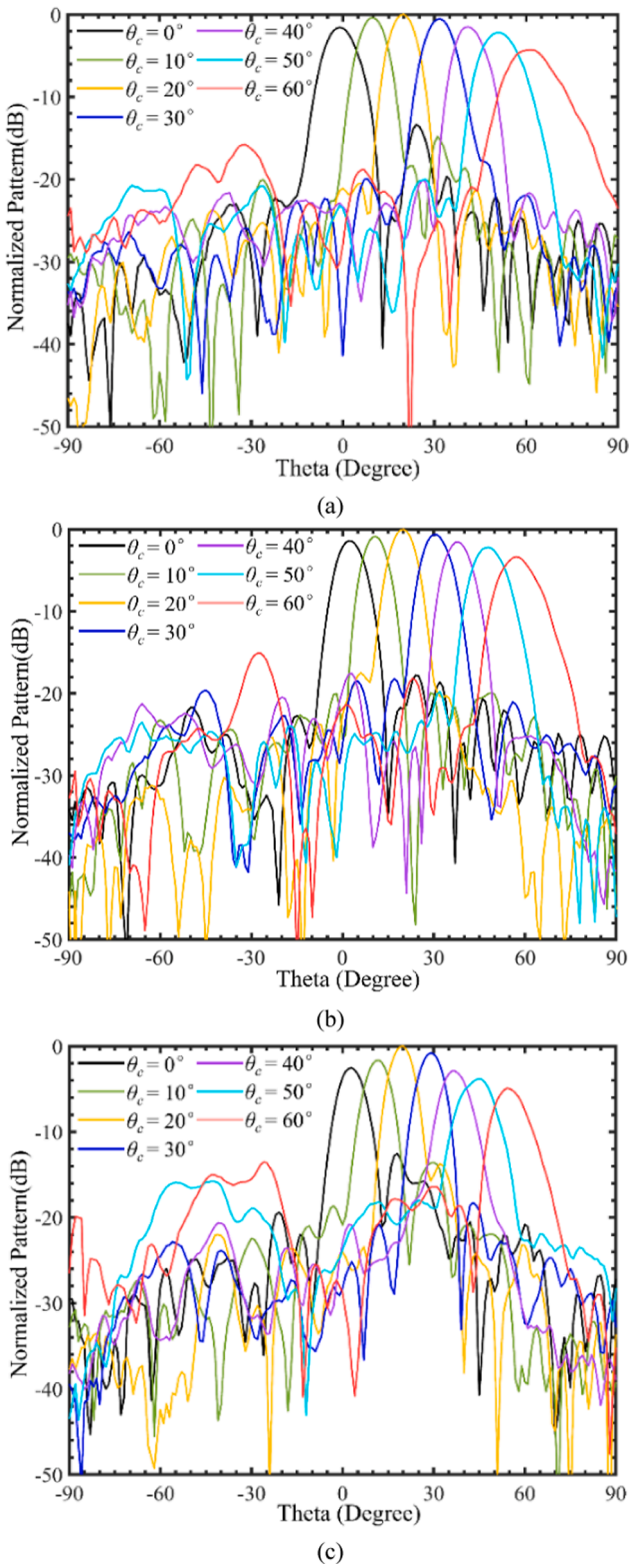

Fig. 9. Measured beam scanning radiation patterns of the RA prototype. The collimation beam is scanned in $\varphi_c = 90°$ plane at (a) 9.5, (b) 10.5, and (c) 11.5 GHz.

can efficiently couple to the waveguide and then for excitation. Additionally, the LSM_{11} mode in Fig. 1(c) reveals the symmetric distribution of the E_y component along the center line parallel to the conductor wall, with equal amplitude and out-of-phase. This observation indicates a canceling effect for cross-polarization, which will be verified by the

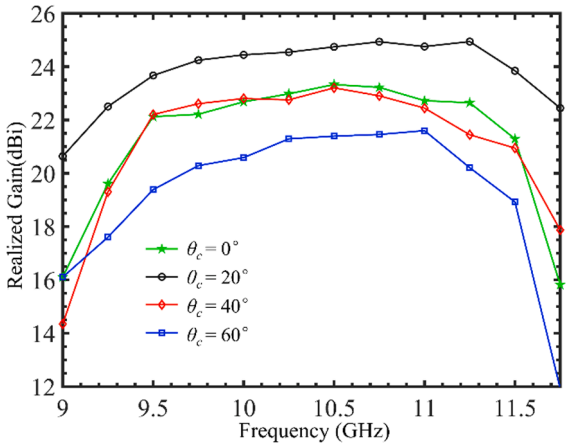

Fig. 10. Measured RA gains in different collimation beam from $\theta_c = 0°$ to 60° at $\varphi_c = 90°$ plane.

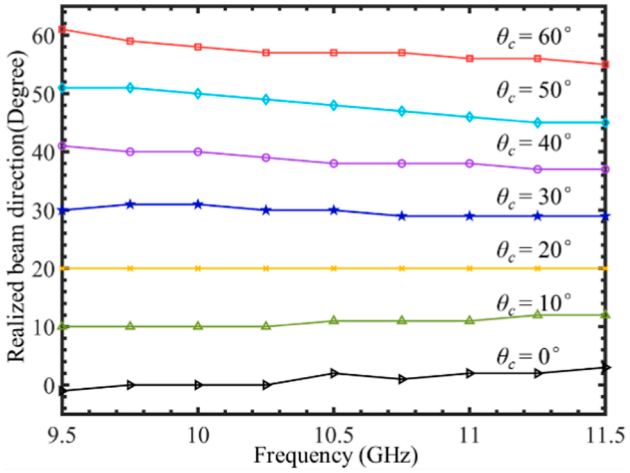

Fig. 11. Measured main beam direction showing the beam squint effect at each designed collimation beam scanning angle.

simulations and measurements in Section III.

For LSM_{11} mode, there are two cutoff frequencies due to the presence of the dielectric slab. The first cutoff frequency, f_1, is associated with the lowest order mode in the Region I, which is the air region surrounding dielectric slab in the waveguide. The second cutoff frequency, f_2, is associated with the single mode in the Region II, which is the region of the waveguide where the dielectric slab is present. The f_1 is determined by the distance a, between the two parallel planes, and its corresponding free space wavelength is $2a$. In contrast, f_2 is determined by the dielectric constant ε_r and the cross-sectional dimensions a and b of the dielectric slab. As the RA unit cell, the single mode bandwidth of the NRD waveguide can be defined as f_1- f_2.

The introduction of air grooves reduces the effective dielectric permittivity of the dielectric slab, leading to a downward shift in the operating frequency and a decrease in the bandwidth. Nevertheless, if the air groove's volume is sufficiently small, the reduction in bandwidth remains within the acceptable range. Considering the difficulty and accuracy of manufacturing, the value of t_b is chosen as 0.8 mm. Table 1 lists all primary dimensions. The periodicity of the proposed unit cell should be 13 mm × 13.3 mm, since the thickness of two metal walls 0.3 mm need to be considered.

The phase tuning can be achieved by changing the insertion depth of the "blade" into the groove. When the blade is inserted into the groove of the dielectric slab, it acts as an additional conductive plate in the middle of the waveguide between the parallel metallic walls. The cutoff frequency f_2 will be increased significantly. As a result, the EM waves propagating in the slab will be reflected by the blade. The phase of the reflected EM wave is determined by the path length before the blade, which is represented by h_r. Fig. 2 depicts the simulation reflection coefficient against the varied length h_r at 10 GHz. The dielectric permittivity used in the simulations is set to 2.7, which is a typical value for polylactide (PLA).

The free space wavelength of the cutoff frequency f_1 should be $2a$ (i.e., 26 mm), corresponding to the frequency of 11.5 GHz. The cutoff frequency f_2 should be high enough so that the reflected waves above this frequency have a sufficient phase shift variation as the value of h_r is changed. Fig. 3 displays the simulation results of the reflection coefficient versus frequency. A frequency of 9.5 GHz is chosen for f_2, as it corresponds to a phase shift of 320° which meets the minimum requirement of the phase tuning in RA unit cell [21]. The magnitude of the reflection coefficient is worse than −1.0 dB at some frequency points within the bandwidth, which is primarily due to the relatively high dielectric loss tangent that we used. The value of f_2 can be further reduced, leading to a wider bandwidth, by utilizing a dielectric material with a higher permittivity for the NRD waveguide. The variation of reflection phase against the position of the inserted blade h_r at different frequencies within the operating bandwidth is shown in Fig. 4. The phase shifting in the NRD waveguide unit cell can be approximated as a linear function of the dielectric slab height h_r, enabling it to function as a transmission line. To minimize the profile, the phase shifting is limited to 360°. As a result, a quasi-time delay (TD) line design is implemented, which approximates the true time delay (TTD) used in wideband operation [22].

Table 2
Comparisons Of The Proposed NRD Waveguide RA with Other Reported Beam scanning RAs and Waveguide RAs.

Ref	Unit cell	Max angle	RA size	F/D	Gain BW (%)	AE BW (%)	X-POL (dB)
[6]	3-layer PCB	45°	10λ diameter	0.85	21(3-dB)	NA	−25
[7]	3-layer PCB	60°	16 × 16 (6λ × 6λ)	1.2	22.3(1-dB)	15 (AE > 20 %)	−28
[8]	Dielectric and metal	60°	25 × 25 (8.7λ × 8.7λ)	0.73	12 (1-dB)	13 (AE > 40 %)	−18
[9]	3-layer PCB	50°	16 × 16 (8λ × 8λ)	0.86	15.4 (1-dB)	NA	−17
[25]	RWG	×	32 × 16 (11λ × 11λ)	0.5	11 (1-dB)	NA	−26.4
[26]	RWG	×	35 × 36 (11.5λ × 11.7λ)	NA	7.4 (1-dB)	NA	NA
This work	NRD waveguide	60°	16 × 16 (8λ × 8λ)	1.22	18(1-dB)	18 (AE > 40 %)	−41

3. Multi-Bit reflectarray antenna design and Measurement

The NRD waveguide based RA is designed with 16 × 16 unit cells. A 15 dBi standard gain horn antenna is chosen as the feed for the RA to avoid the complex feed system for waveguide radiator [23], following the design of most RA. The feed is offset by 20° to the broadside on the *yoz* plane and the F/D value is set to 1.07. The power taper in the x-direction is −10 dB, while in the y-direction, the power taper is −12 dB and −8 dB at the far and near edges, respectively. By adjusting the position of the inserted blade h_r in each unit cell, the reflection phase can be controlled to achieve the desired compensation phase using the equation:

$$\phi_{com} = -2\beta \bullet h_r + \phi_0 \tag{1}$$

where β is the propagation constant of the NRD waveguide and ϕ_0 is a constant phase offset. At the center frequency of 10.5 GHz, the values of β and ϕ_0 are evaluated by Fig. 4 as 11 and 190, respectively. Finally, for the collimation beam with (θ_c, φ_c), the required value of h_r for the (m,n)-*th* unit cell can be calculated by:

$$h_r = \frac{\phi_0 - \phi_{ref} - k_0 r_{mn} - \phi_{mn}}{2\beta} \tag{2}$$

where k_0 presents the free space wavenumber of incident wave, ϕ_{ref} is a reference phase for optimization of RA performance, r_{mn} is the distance from the feed's phase center to the (m, n)-*th* unit cell. ϕ_{mn} is progressive phase. It should be noted that the value of ϕ_{ref} is chosen within the range of (-640°, −280°) to optimize the gain flatness of the RA [72124]. To verify the beam scanning capabilities, a RA with 16 × 16 unit cells is designed with collimation beam starting from $\theta_c = 0°$ and sweeping up to $\theta_c = 60°$ in 10° increments at the $\varphi_c = 90°$ plane. Fig. 5 shows the fabricated prototype with collimation beam at $\theta_c = 30°$ and $\varphi_c = 90°$ direction.

The H-plane radiation pattern is initially measured by rotating in the *yoz* plane, as depicted in Fig. 6. The E-plane radiation pattern will be scanned in a plane perpendicular to the *yoz* plane passing through the direction of maximum radiation. Fig. 7 presents a comparison between the measured and simulated results for gain with collimation beam at 20°. The measured 1-dB gain bandwidth is 18 % with a peak gain value of 24.9 dBi. Furthermore, the aperture efficiency exceeds 40 % within this bandwidth. Fig. 8 depicts the comparisons between measured and simulated radiation patterns at the center frequency of 10.5 GHz. The measured radiation pattern closely corresponds to the simulated results. The side lobe level (SLL) in both the H-plane and E-plane is approximately −20 dB. The cross-polarization (X-POL) level remains below −38 dB in the main beam direction.

The measured beam scanning performance is demonstrated in Figs. 9 and 10. The aperture blockage effect is relatively significant when the collimation beam is at 0° and 10°, but the realized gain will be reduced and the SLL will be increased when comparing to the values observed at 20°. When the collimated beam is scanned to 60°, there is an average scanning loss of 3.5 dB, while still ensuring sidelobe levels (SLL) below −10 dB and cross-polarization (X-POL) levels below −25 dB. Moreover, the 1.0-dB gain bandwidth remains consistently above 14 %. As shown in Fig. 11, the maximum beam squint is 6° at the higher edge of the frequency band which is relatively small compared with other reported beam-steerable RAs because the quasi-TD line design partially mitigates the beam squint effect. Table 2 provides a comparison of the measured performance of the proposed NRD waveguide RA prototype with other reported wideband beam scanning RAs and waveguide type RAs. The results indicate that the proposed RA has significant advantages in terms of gain bandwidth with improved efficiency. Moreover, the proposed RA exhibits low X-POL values, benefiting from its waveguide-type structure.

4. Conclusion

A wideband multi-bit RA based on NRD waveguide has been designed and experimentally verified. Due to the wideband feature of the proposed NRD waveguide unit cell, the RA offers significant advantages of wide bandwidth for all collimation beams, which proves the suitability of NRD waveguides for beam-scanning wideband RA applications with low cross-polarization and low metal loss. The reconfigurable for real-time beam scanning can be achieved by mechanical methods, such as micro motors or magnetostatics [27].

CRediT authorship contribution statement

Wen Wu: Writing – original draft, Conceptualization. **Kai-Da Xu:** Writing – review & editing, Supervision. **Daotong Li:** Formal analysis. **Qiang Chen:** Supervision.

Declaration of competing interest

The authors declare that they have no known competing financial interests or personal relationships that could have appeared to influence the work reported in this paper.

This work was supported by the Guangxi Key Laboratory of Wireless Broadband Communication and Signal Processing under Grant GXKL06220203.

Data availability

Data will be made available on request.

References

[1] Otsuji T, Iwatsuki K, Yamada H, Yashima M. Concept of resilient electric power and information communication technology (R-EICT) converged network systems based on overall optimization of autonomous decentralized cooperative control of DC microgrids. IEEE Power & Energy Society Innovative Smart Grid Technologies Conference (ISGT) 2021;2021:1–5.
[2] Tanaka T, Minami H, et al. "Energy-distribution platform technologies toward zero environmental impact"+. NTT Technical Review 2021;19(6).
[3] Wu W, Xu K-D, Chen Q, Tanaka T, Kozai M, Minami H. A wideband reflectarray based on single-layer magneto-electric dipole elements with 1-bit switching mode. IEEE Trans Antennas Propag 2022;70(12):12346–51.
[4] Cao X, Chen Q, Tanaka T, Kozai M, Minami H. A 1-bit time-modulated reflectarray for reconfigurable-intelligent-surface applications. IEEE Trans Antennas Propag 2023;71(3):2396–408.
[5] Nayeri P, Yang F, Elsherbeni AZ. Beam–scanning reflectarray antennas: A technical overview and state of the art. IEEE Antennas Propag Mag 2015;57(4):32–47.
[6] Luyen H, Booske JH, Behdad N. 2-bit phase quantization using mixed polarization-rotation/non-polarization- rotation reflection modes for beam-steerable reflectarrays. IEEE Trans Antennas Propag 2020;68(12):7937–46.
[7] Xiang BJ, Dai X, Luk K-M. A wideband low-cost reconfigurable reflectarray antenna with 1-bit resolution. IEEE Trans Antennas Propag 2022;70(9):7439–47.
[8] Xu L, Yuan C, Zhang Q, Liu J, Zhang Q, Sun Y. Design and experiments of a beam-steerable wideband reflectarray antenna for high-power microwave applications. IEEE Trans Antennas Propag 2023;71(2):1955–9.
[9] Yang YS, Guan DF, Fu YF, Gu ZY, Zhang JD, Qian ZP, et al. Broadband huygens resonance transmitarray based on lightweight polyimide membrane. IEEE Antennas Wireless Propag Lett 2024;23(3):1035–9.
[10] Flamini R, et al. Toward a heterogeneous smart electromagnetic environment for millimeter-wave communications: An industrial viewpoint. IEEE Trans Antennas Propag 2022;70(10):8898–910.
[11] Nayeri P, et al. 3D printed dielectric reflectarrays: Low-cost high-gain antennas at sub-millimeter waves. IEEE Trans Antennas Propag 2014;62(4):2000–8.
[12] Wu MD, Li B, Zhou Y, Guo DL, Liu Y, Wei F, et al. Design and measurement of a 220 GHz wideband 3-D printed dielectric reflectarray. IEEE Antennas Wireless Propag Lett 2018;17(11):20942098.
[13] Zheng Z, Zhang L, Luo Q, Mao C, He Y, Gao S. Wideband 3D-printed transmit-reflect-array antenna with independent beam control. IEEE Trans Antennas Propag 2023;71(7):6196–201.
[14] Zhu J, Yang Y, Mcgloin D, Liao S, Xue Q. 3-D printed all-dielectric dual-band broadband reflectarray with a large frequency ratio. IEEE Trans Antennas Propag 2021;69(10):7035–40.
[15] Yoneyama T, Nishida S. Non-Radiative dielectric waveguide for millimeter-wave integrated circuits. IEEE Trans Microwave Theory Tech 1981;vol MTT-29:1188–92.

[16] Dallaire J, Wu K. Complete characterization of transmission losses in generalized nonradiative dielectric (NRD) waveguide. IEEE Trans Microwave Theory Tech 2000;48(1):121–5.
[17] Wu W, Xu K-D, Chen Q, Tanaka T, Kozai M, Minami H. A low-cost wideband reflectarray antenna based on nonradiative dielectric waveguide. IEEE Antennas Wireless Propag Lett 2023;22(12):3152–6.
[18] Berry D, Malech R, Kennedy W. The reflectarray antenna. IEEE Trans Antennas Propag 1963;11(6):645–51. https://doi.org/10.1109/TAP.1963.
[19] Mondal P, Wu K. Single mode operation of substrate integrated non-radiative dielectric waveguide and an excitation scheme of LSE_{11} mode. IEEE Microw Wireless Compon Lett 2013;23(8):418–20.
[20] Kuroki F, Ikeda K, Matsukawa T. Transmission characteristics of LSE/sub 01/ mode in high permittivity NRD guide. Proceedings of 1997 Asia-Pacific Microwave Conf 1997;2:593–6.
[21] Nayeri P, Yang F, Elsherbeni AZ. Reflectarray antennas: Theory, designs, and applications. Hoboken, NJ, USA: Wiley; 2018.
[22] Carrasco E, Encinar JA, Barba M. Bandwidth improvement in large reflectarrays by using true-time delay. IEEE Trans Antennas Propag 2008;56(8):2496–503.
[23] Chen Z, Guan Dongfang, Qian Z, Wu W. Dual-polarized siw leaky-wave antenna based on mode-multiplexed feeding structure. IEEE Antennas Wireless Propag Lett, Jan 2023;22(1):104–8.
[24] Mao Y, Xu S, Yang F, Elsherbeni AZ. A novel phase synthesis approach for wideband reflectarray design. IEEE Trans Antennas Propag 2015;63(9):4189–93.
[25] Wu G-B, Zeng Y-S, Chan KF, Chen B-J, Qu S-W, Chan CH. High-gain filtering reflectarray antenna for millimeter-wave applications. IEEE Trans Antennas Propag 2020;68(2):805–12.
[26] Liu Y, Cheng YJ, Zhao M-H, Fan Y. Dual-band shared-aperture high-efficiency reflectarray antenna based on structure-reuse technique. IEEE Antennas Wireless Propag Lett 2021;20(3):366–70.
[27] Hu A, Konno K, Chen Q, Takahashi T. A highly efficient 1-bit reflectarray antenna using electromagnet-controlled elements. IEEE Trans Antennas Propag 2024;72(1):506–17.